Version: Published in: Proc. Roy. Soc. London A, vol. 461, pp. 79-97 (2005)

Wetting of rough surfaces: a homogenization approach

Giovanni Alberti, Antonio DeSimone

Abstract: The contact angle of a drop in equilibrium on a solid is strongly affected by the roughness of the surface on which it rests. We study the roughness-induced enhancement of the hydrophobic or hydrophilic properties of a solid surface through homogenization theory. By relying on a variational formulation of the problem, we show that the macroscopic contact angle is associated with the solution of two cell problems, giving the minimal energy per unit macroscopic area for a transition layer between the rough solid surface and a liquid or vapor phase. Our results are valid for both chemically heterogeneous and homogeneous surfaces. In the latter case, a very transparent structure emerges from the variational approach: the classical laws of Wenzel and Cassie-Baxter give bounds for the optimal energy, and configurations of minimal energy are those leading to the smallest macroscopic contact angle in the hydrophobic case, to the largest one in the hydrophilic case.

Keywords: wetting, contact angle, rough surfaces, homogenization, calculus of variations, geometric measure theory.

Mathematics Subject Classification (2000): 76B45 (74Q05, 49J45, 49Q10, 49Q20)

Physics and Astronomy Classification Scheme (2003): 68.08.Bc, 68.03.Cd, 47.55.Dz

1. Introduction

The study of the wetting properties of rough surfaces has attracted considerable attention in the last few years, see [6], [13] and the many references quoted therein. Although some key theoretical and experimental contributions are already a few decades old ([23], [8], [15]), a noticeable surge of interest in the Soft Matter Physics literature seems correlated with the recent studies on the superhydrophobic properties of the leaves of some plants, see [18], [19]. The basic observation is that, when the surfaces of the leaves are rough at a microscopic scale, macroscopic drops sitting on the leaves do not wet them (this effect is displayed also by artificial surfaces – see, e.g., Figure 1 and [17]).

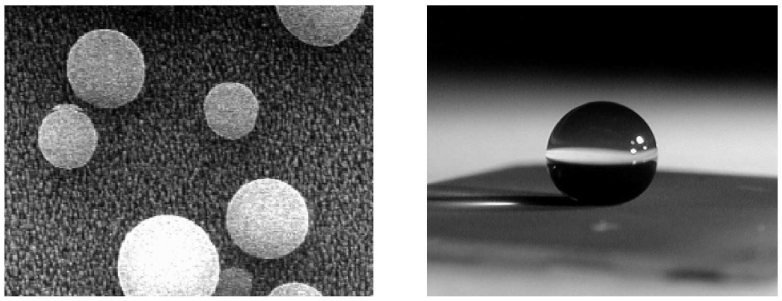

Fig. 1. Drops of water on a carpet of vertically aligned carbon nanotubes at different magnifications. The drop diameters are approximately 5 to 10 μm in the left panel, 5 mm in the right panel (micrographs courtesy of Prof. G.H. McKinley, MIT).

The most basic route towards explaining the observed shapes of equilibrium drops on rough surfaces is based on energy minimization and separation of scales between the size of the drops and that of the asperities. Minimization of the total interfacial energy of a system composed of a liquid drop (phase L), a solid substrate (phase S), and a vapor environment (phase V)

$$E = \sigma_{SL}|\Sigma_{SL}| + \sigma_{SV}|\Sigma_{SV}| + \sigma_{LV}|\Sigma_{LV}|$$

leads to the classical Young law for the contact angle θ

$$\cos\theta = \frac{\sigma_{SV} - \sigma_{SL}}{\sigma_{LV}},$$

see Figure 2 below. Here Σ_{AB} is the interface between phases A and B, $|\Sigma_{AB}|$ is its area, and σ_{AB} is the corresponding interfacial energy density. A hydrophobic (respectively, hydrophilic) surface is one for which $\cos\theta$ is negative (respectively, positive), and it is commonly observed that, by micro-texturing a surface to increase its roughness, one causes the contact angle to increase in the hydrophobic case, decrease in the hydrophilic one. The effect of microscopic surface roughness on the macroscopic contact angle is easily understood if one realizes that the actual (microscopic) area of contact may differ from the one that is apparent at the macroscopic scale. To keep this into account, it is necessary to renormalize the coefficients σ_{SL} and σ_{SV}. The macroscopic contact angle $\theta^{\rm hom}$ is thus given by

$$\cos\theta^{\rm hom} = \frac{\sigma^{\rm hom}_{SV} - \sigma^{\rm hom}_{SL}}{\sigma_{LV}},$$

where $\sigma^{\rm hom}_{SV}$ (respectively, $\sigma^{\rm hom}_{SL}$) represents the minimal energy per unit macroscopic area for a transition layer between a microscopically rough solid and the vapor phase (respectively, the liquid phase). Clearly, this argument lends itself to homogenization theory, and this is precisely the approach followed in this paper. In fact, we show that $\theta^{\rm hom}$ can be characterized as the contact angle for a minimizer of the "homogenized" energy

$$E^{\rm hom} = \sigma^{\rm hom}_{SL}|\Sigma_{SL}| + \sigma^{\rm hom}_{SV}|\Sigma_{SV}| + \sigma_{LV}|\Sigma_{LV}|\ .$$

The key step in the computation of $\cos\theta^{\rm hom}$ is thus the solution of two well defined variational problems (cell problems), leading to the determination of the effective energy densities $\sigma^{\rm hom}_{SV}$ and $\sigma^{\rm hom}_{SL}$.

Seen from our perspective, the classical contributions from the Physics literature can be interpreted as attempts to construct energy minimizing configurations based on a good physical intuition of the possible geometries for the microscopic contacts. In fact, based on two different hypotheses for the underlying contact mechanisms, two antagonistic models have emerged, leading to two different predictions for the macroscopic contact angle $\theta^{\rm hom}$. Assuming that contact between liquid and solid is maintained at every point of the rough surface (complete contact), one obtains the so-called Wenzel law [23], which in the hydrophobic case predicts an amplification of the contact angle which only depends on the ratio R between actual (microscopic) and apparent (macroscopic) contact area.

Assuming instead that vapor fills the bottom of the asperities of a rough surface (composite contact), one obtains the so called Cassie-Baxter law [8] which, unless $\cos\theta$ is sufficiently small, gives a less spectacular roughness-induced enhancement of the hydrophobicity of a surface when compared to Wenzel's predictions. Only very recently it

has been recognized that, of the two proposed mechanisms, only one at a time can lead to a minimum energy configuration [5], [20]. Actually, as an example of the results that our homogenization approach easily delivers, it can be shown that the minimal energy configuration is always the one corresponding to the most conservative estimate of the roughness-induced enhancement of the hydrophobic or hydrophilic properties of a surface,[(1)] and that in certain cases, both Wenzel and Cassie-Baxter laws overestimate this effect. These and other results of physical relevance are discussed in detail in Section 4.

The debate over which model, whether Wenzel's or Cassie-Baxter's is the appropriate one, is just one example of issues on which a general consensus of opinion has not yet emerged in the literature. Other examples are the question of whether the relation between $\cos\theta^{\rm hom}$ and $\cos\theta$ should be symmetric when going from the hydrophilic to the hydrophobic regime (see, e.g., [4]), or the claim that a fractal surface with a hierarchy of roughness scales may lead to further enhancement of hydrophobicity, and even make hydrophobic a surface made of a hydrophilic material [14]. Some of these statements arise from the need of explaining experimental observations, while others are of a more speculative nature. Our results show that, within the class of energy minimizing configurations, the relation between $\cos\theta^{\rm hom}$ and $\cos\theta$ is always symmetric and, moreover, it is not possible to turn a hydrophilic surface into a hydrophobic one by simply tuning its roughness (see the discussion in Subsection 4.7). Of course, these statements should be taken with a grain of salt. While equilibrium configurations which are not energy minimizers are only metastable, and hence somewhat volatile, they are actually observable. By examining the consequences that can be deduced from energy minimization and separation of scales, we hope to help clarifying which aspects of the available experimental evidence are associated with energetics, and which ones should be instead attributed to different mechanisms (switching among multiple equilibria, metastability and hysteresis, dynamic effects). In particular, we can conclude that both the experimentally observed lack of symmetry in the relation between $\cos\theta^{\rm hom}$ and $\cos\theta$, and the fact that drops sitting on hydrophilic rough surfaces may exhibit large contact angles are manifestations of metastability.

It is worth emphasizing that our approach is entirely based on minimization of the total interfacial energy, while most of the Physics literature is based on constructing equilibrium configurations satisfying the contact angle condition given by Young's law (a different point of view, based on Statistical Mechanics is also being pursued, see e.g. [22]). There is clearly no difference in the underlying physical model, in the sense that the equilibrium configurations mentioned above are exactly the critical points of the energy we use, see the discussion in Section 2. In restricting attention to energy minimizers we accept to overlook metastable equilibria (even though some of our homogenization results should remain valid even in this context). The reason for our choice is that the variational structure is extremely useful in building a coherent conceptual framework of the phenomena under study. First, it gives us a precise formulation of the problem to be solved for situations, such as that of a rough and chemically heterogeneous solid, where an approach based on direct geometric constructions would be unfeasible. Even more importantly, for the easier case of a chemically homogeneous solid, the variational approach is very effective in reducing the essentials of the problem to a few, very transparent basic

(1) A similar conclusion is reached in [20]. There, only Wenzel and Cassie-Baxter configurations are compared while, in our analysis, arbitrary test configurations are allowed to compete for minimal energy.

facts, which are summarized below.

Through a straightforward renormalization of the interfacial energy, one shows that $|\cos\theta^{\rm hom}|$ is the energy per unit apparent area of the optimal transition layer between a rough solid and a liquid (hydrophobic case) or a vapor (hydrophilic case) phase. By looking for bounds for the optimal energy through the use of trial configurations (e.g., based on models for the geometry of the microcontacts), the classical results from the Physics literature can be recovered in a systematic way. The conditions under which the Wenzel ansatz of complete contact, or the Cassie-Baxter ansatz of composite contact provide energetically optimal configurations can be scrutinized. The criterion that lowest energy is associated with smallest $|\cos\theta^{\rm hom}|$ (i.e., with the most conservative estimate of the roughness-induced enhancement of the hydrophobic or hydrophilic properties of a surface) emerges naturally.

Finally, we point out that our mathematical result consists in computing a limit energy as a certain parameter ε, representing the length–scale of roughness relative to that of the droplets, tends to 0. The resulting model should be applicable to drops that are large compared to the typical size of the asperities, but we have no quantitative estimate of the scale at which the limit model becomes reliable. Even the micron–sized droplets of Figure 1 seem to conform well to the predictions based on the limit energy. There are, however, recent observations of sub–micron droplets where super–hydrophobicity seems suppressed ([9], see also [21]). For these, the model based on the limit energy is no longer applicable.

The rest of this paper is organized as follows. In Section 2 the variational formulation of the problem and the corresponding necessary conditions for critical points are reviewed. In Section 3 a non-technical statement of our homogenization result is given, and its physical implications are discussed in Section 4. Section 5 contains the rigorous mathematical statements of our results and the corresponding proofs.

2. Energy and equilibrium conditions

We denote by S, L, and V the three regions of $\mathbb{R}^d$ $(d = 2, 3)$ occupied by solid, liquid, and vapor phase. The first one is a given, nice closed set, possibly unbounded. The other two are the unknowns of the problem.

We are interested in minimizing the following interfacial energy

$$E = \sigma_{SL}|\Sigma_{SL}| + \sigma_{SV}|\Sigma_{SV}| + \sigma_{LV}|\Sigma_{LV}| \quad + [\text{a.t.}], \tag{2.1}$$

where [a.t.] indicates the fact that additional integral terms or constraints may be present; Σ_{AB} is the interface of phases A and B, $|\Sigma_{AB}|$ denotes its measure. The (positive) material parameters σ_{AB} (called surface tensions, or interfacial energies densities) satisfy the *wetting condition*

$$|\sigma_{SL} - \sigma_{SV}| \leq \sigma_{LV} \ . \tag{2.2}$$

2.1. Additional terms and constraints. - A typical example of [a.t.] is the potential energy due to gravity, namely

$$\gamma \int_L h \tag{2.3}$$

where $\gamma > 0$ is the difference between the specific gravities of L and V, and $h(x)$ is the height of point x. Another example is a constraint on the volume of L, namely

$$|L| = l \tag{2.4}$$

with l a given positive number.

It is important to notice that the analysis that follows is not affected by the presence of such terms (cf. §2.4)

2.2. Chemically heterogeneous surfaces. - For a solid S with a chemically heterogeneous surface, σ_{SL} and σ_{SV} are functions defined on ∂S (and satisfying (2.2)). In this case, the interfacial energy becomes

$$E := \int_{\Sigma_{SL}} \sigma_{SL} \; + \int_{\Sigma_{SV}} \sigma_{SV} \; + \sigma_{LV}|\Sigma_{LV}| \quad + [\text{a.t.}]. \tag{2.5}$$

2.3. Energy renormalization. - Since $|\Sigma_{SV}| + |\Sigma_{SL}| = |\partial S|$ is fixed, if needed, we can always renormalize the energy E in (2.1) by subtracting a constant c times $|\Sigma_{SV}| + |\Sigma_{SL}|$, In other words, the configurations of minimal energy are unaffected by the substitution

$$(\sigma_{LV}, \sigma_{SV}, \sigma_{SL}) \to (\sigma_{LV}, \sigma_{SV} - c, \sigma_{SL} - c) \; .$$

The same argument applies to the energy in (2.5); in fact we can even subtract a non-constant function c. Moreover the minimizers of E are also invariant under the substitution

$$(\sigma_{LV}, \sigma_{SV}, \sigma_{SL}) \to (\alpha\sigma_{LV}, \alpha\sigma_{SV}, \alpha\sigma_{SL})$$

where α is any positive real number (in this case, the eventual additional term [a.t.] must be modified accordingly).

Assume now that σ_{SV} and σ_{SL} are constant, and define the angle $\theta \in [0, \pi]$ by

$$\cos\theta := \frac{\sigma_{SV} - \sigma_{SL}}{\sigma_{LV}} \tag{2.6}$$

(the right-hand side of (2.6) belongs to $[-1, 1]$ because of the wetting condition (2.2), and therefore the angle θ is well-defined; its physical meaning is explained in §2.4 below). So, if $\sigma_{SV} \geq \sigma_{SL}$, we can use the substitution $(\sigma_{LV}, \sigma_{SV}, \sigma_{SL}) \to (1, \cos\theta, 0)$ and reduce to an interfacial energy of the form

$$\tilde{E} = \cos\theta \, |\Sigma_{SV}| + |\Sigma_{LV}| \quad + [\text{a.t.}] \tag{2.7}$$

Similarly, if $\sigma_{SV} \leq \sigma_{SL}$, we substitute $(\sigma_{LV}, \sigma_{SV}, \sigma_{SL}) \to (1, 0, |\cos\theta|)$ and reduce to

$$\tilde{E} = |\cos\theta| \, |\Sigma_{SL}| + |\Sigma_{LV}| \quad + [\text{a.t.}] \tag{2.8}$$

These renormalized energies show that, besides the physical parameters appearing in [a.t.], the only relevant physical parameter in the problem is $\cos\theta$. When $\cos\theta$ is positive, energy minimization promotes maximization of the area of Σ_{SL} at the expenses of Σ_{SV} and ∂S is called a hydrophilic surface. When $\cos\theta$ is negative, energy minimization promotes minimization of Σ_{SL} and ∂S is called hydrophobic.

We now proceed towards reviewing some classical (equilibrium) conditions which are necessarily satisfied by critical points of E (see, e.g., [11]). To keep technical details to a minimum, we will tacitly assume that the sets S, L, and V are as regular as needed to grant a meaning to the notions of interface normal, curvature, etc.

2.4. Contact angle and Young's law. - The vapor-liquid interface Σ_{VL} meets the solid surface ∂S with a contact angle which is equal to the angle θ given by (2.6) – see Figure 2, left. This relation is known as Young's law.

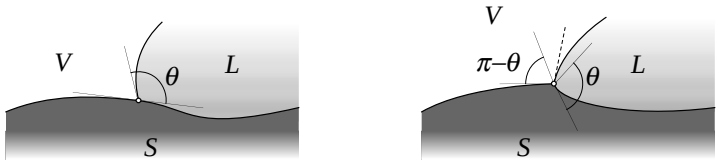

Fig. 2. Geometry of S-V-L contact, and Young's law.

It may happen that the contact line where Σ_{VL} meets ∂S coincides (partly) with a convex edge of ∂S; in this case the contact angle belongs to the interval described in Figure 2, right. On the other hand, Σ_{VL} never meets ∂S along a concave edge (more precisely, the contact line and a concave edge can only intersect transversally). We emphasize that Young's law is valid with or without a volume constraint, and with or without the presence of a potential energy.

2.5. Curvature equation. - The mean curvature H of the vapor-liquid interface Σ_{VL} satisfies

$$2H = \lambda + \frac{\gamma h}{\sigma_{VL}} \tag{2.9}$$

where the scalar λ is a constant Lagrange multiplier, which is present only in association with the volume constraint (2.4), while the second summand on the right-hand side is present only in association with the potential energy (2.3).

3. The homogenization formula

We assume that the solid surface is macroscopically flat and coincides with the "horizontal" plane $x_d = 0$, and it is rough at a scale ε, where ε is a positive scaling parameter. More precisely, we assume that S_ε is of the form

$$S_\varepsilon := \{\varepsilon x : \ x \in S_1\} \ , \tag{3.1}$$

where S_1 is a closed set in $\mathbb{R}^d$ such that $\{x_d \le 0\} \subset S \subset \{x_d \le a\}$ for some $a > 0$, it is *r-periodic* in the first $d-1$ directions for some $r > 0$ (i.e., invariant under translation by re_i for $i = 1, \dots, d-1$), and *symmetric* with respect to the coordinate planes $x_i = 0$ for $i = 1, \dots, d-1$. For example, one can take S_1 equal to the subgraph of a positive bounded function f of the first $d-1$ variables which is *r-periodic and even*, so that

$$S_\varepsilon = \left\{x_d \le \varepsilon f(x_1/\varepsilon, \dots, x_{d-1}/\varepsilon)\right\} \ . \tag{3.2}$$

In the limit $\varepsilon \to 0$, the sets S_ε converge to the half-space $S := \{x_d \leq 0\}$, and energy minimizing configurations are obtained by minimizing the homogenized energy

$$E^{\hom} := \sigma_{SL}^{\hom}|\Sigma_{SL}| + \sigma_{SV}^{\hom}|\Sigma_{SV}| + \sigma_{LV}|\Sigma_{LV}| \quad + [\text{a.t.}]; \tag{3.3}$$

the energy density $\sigma_{SL}^{\hom}$ is obtained by solving the cell problem

$$\sigma_{SL}^{\hom} := \inf_V \frac{E(V, C_r)}{|Q_r|} \ , \tag{3.4}$$

where Q_r is the square of all x in the plane $x_d = 0$ such that $-r/2 < x_i < r/2$ for $i = 1, \ldots, d-1$, C_r is the open cylinder $Q_r \times \mathbb{R}$, $E(V, C_r)$ denotes the energy associated to a test set V within the periodicity cell C_r, with *no additional term*, and the infimum is taken over all bounded sets V contained in $C_r \setminus S_1$ which are symmetric with respect to the coordinate planes $x_i = 0$ for $i = 1, \ldots, d-1$. Similarly, $\sigma_{SV}^{\hom}$ is given by the cell problem

$$\sigma_{SV}^{\hom} := \inf_L \frac{E(L, C_r)}{|Q_r|} \ . \tag{3.5}$$

The macroscopic contact angle is then given by the formula

$$\cos\theta^{\hom} = \frac{\sigma_{SV}^{\hom} - \sigma_{SL}^{\hom}}{\sigma_{LV}} \ . \tag{3.6}$$

3.1. REMARKS. - (i) Formula (3.3) will be rigorously justified in term of Γ-convergence in Theorem 5.2.

(ii) In the minimization problem (3.4) amounts to finding the (energetically) more convenient way to interpose a vapor layer between the given solid phase S_1 and the liquid phase, within the periodicity cell C_r (see Figure 3 below). Similarly, problem (3.4) amounts to finding the more convenient way to make a transition from solid to vapor. In the hydrophilic case the best transition from solid to liquid is obtained for V empty, that is, it is not convenient to insert any vapor layer, while in the hydrophobic case the best transition from solid to vapor is obtained for L empty.

(iii) Let P_a be a closed half-space of the form $x_d \leq a$ that contains S_1. It is easy to show that the total capillary energy of $V \cap P_a$ is not larger than that of V, and therefore one can freely add to the cell problem (3.4) the constraint $V \subset P_a$. The same for the cell problem (3.5).

(iv) The energy densities $\sigma_{SL}^{\hom}$ and $\sigma_{SV}^{\hom}$ satisfy the wetting condition

$$|\sigma_{SL}^{\hom} - \sigma_{SV}^{\hom}| \leq \sigma_{LV} \ .$$

Hence the right-hand side of (3.6) belongs to $[-1, 1]$ and $\theta^{\hom}$ is a well-defined angle between 0 and π. Indeed, given a configuration which makes the transition from solid to liquid (the one tested in (3.5)), by adding a flat interface from liquid to vapor, we obtain a new configuration which makes the transition from solid to vapor, and whose energy is that of the previous configuration plus $\sigma_{LV}|Q_r|$. Hence $\sigma_{SV}^{\hom} \leq \sigma_{SL}^{\hom} + \sigma_{LV}$. In a similar way we prove that $\sigma_{SL}^{\hom} \leq \sigma_{SV}^{\hom} + \sigma_{LV}$.

(v) The periodicity assumption on S_1 and the scaling formula (3.1)) encode our idea of a flat surface with roughness on a small scale. The symmetry assumption on S_1 has

a purely technical meaning; if removed, the formulas for the homogenized coefficients becomes more complicated (cf. Theorem 5.2).

(vi) Formulas (3.4) and (3.5) hold even for surfaces which are chemically heterogeneous on the same scale of the roughness. More precisely, we assume that the solid-liquid and the solid-vapor energy densities depend on ε and are of the form

$$\sigma^{\varepsilon}_{SL}(x) := \sigma_{SL}(x/\varepsilon) \ , \ \sigma^{\varepsilon}_{SV}(x) := \sigma_{SV}(x/\varepsilon) \ , \tag{3.7}$$

where σ_{SL} and σ_{SV} are r-periodic even functions defined on S_1. In case S_1 is flat (no roughness), the minima in (3.4) and (3.5) are achieved respectively for V and L empty, and therefore $\sigma^{\rm hom}_{SL}$ and $\sigma^{\rm hom}_{SV}$ are the average of σ_{SL} and σ_{SV} on the periodicity cell.

3.2. Explicit computations in dimension $d = 2$. - The homogenized coefficients are in general hard to compute. However, we notice that the infimum in (3.4) (resp., (3.5)) is always achieved, and the optimal V satisfy Young's law and the liquid-vapor interface Σ_{LV} has zero mean curvature (in the cell problem (3.4), the volume of V is not constrained). In dimension $d = 2$, this means that Σ_{LV} is made of line segments which meet the solid surface with given angle θ. In general, this allows only for a finite number of possible configurations, that can be easily guessed and checked one by one for optimality (see Figure 3).

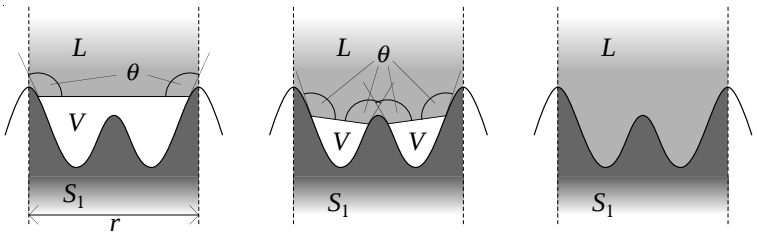

Fig. 3. Possible optimal configurations for a two-dimensional geometry (hydrophobic case).

In dimension $d = 3$, these computations become unfeasible because there are many more surfaces with zero mean curvature than just planes.

4. Discussion of the physical implications

A typical way of investigating experimentally the wetting properties of rough surfaces is to determine, for a fixed surface, the macroscopic contact angle for various liquids in a controlled atmosphere. This amounts to plotting $\cos\theta^{\rm hom}$ as a function of $\cos\theta$, at fixed S_1.

A first result of our analysis is that such diagram is symmetric, that is, $\cos\theta^{\rm hom}$ is an odd function of $\cos\theta$. This is because the solution corresponding to a sign change of $\cos\theta$ can be obtained by exchanging the role of L and V in (3.4) and (3.5). The two values of $\sigma^{\rm hom}_{SL}$ and $\sigma^{\rm hom}_{SV}$ are thus exchanged, leading to a change of sign of $\cos\theta^{\rm hom}$. The physical implication is that deviations from symmetry of experimental plots of $\cos\theta^{\rm hom}$ vs. $\cos\theta$ cannot be attributed to energy minimizing properties of rough surfaces, but rather to

the fact that experimental measurements are affected by multiplicity of metastable equilibrium configurations, hysteresis, dynamical effects.

In the rest of this section, we will restrict our attention to the case of chemically homogeneous solid phase, described by (3.2), and satisfying symmetry condition described in Section 3. This is the case that has received most attention in the Physics literature. A crucial parameter is then the ratio R between effective and apparent area of the solid surface, that is

$$R := \frac{|\partial S_1 \cap C_r|}{|Q_r|} \ , \tag{4.1}$$

where Q_r and C_r are defined as in Section 3. If S_1 is the subgraph of a sufficiently regular function f (see (3.2)), then R is given by the formula

$$R = \frac{1}{|Q_r|} \int\limits_{Q_r} \sqrt{1 + |\nabla f|^2} \ ,$$

Thus R gives a quantitative measure of the roughness of the reference surface ∂S_1 and of all its scaled copies ∂S_ε.

The hydrophilic case

Throughout this subsection, we assume $\cos\theta \geq 0$, and replace the interfacial energy E with the renormalized energy $\tilde{E}$ in (2.7). Thus the energy that appears in the cell problems (3.4) and (3.5) is

$$\tilde{E}(L, C_r) = \tilde{E}(V, C_r) = \cos\theta \, |\Sigma_{SV}| + |\Sigma_{LV}| \ ,$$

and one immediately verifies that the infimum in (3.4) is achieved for V empty, that is, $\tilde{\sigma}_{SL}^{\rm hom} = 0$ (see Remark 3.1(ii)). Hence (3.5) becomes

$$\cos\theta^{\rm hom} = \tilde{\sigma}_{SV}^{\rm hom} = \inf_L \frac{1}{|Q_r|} \tilde{E}(L, C_r) \ . \tag{4.2}$$

4.1. Roughness enhances hydrophily. - For hydrophilic surfaces, roughness decreases the contact angle, that is,

$$\cos\theta \leq \cos\theta^{\rm hom} \ .$$

This inequality is a consequence of the following estimate: for every admissible set L for the minimum problem (4.2) there holds

$$\begin{aligned} \tilde{E}(L, C_r) &= \cos\theta |\Sigma_{SV}| + |\Sigma_{LV}| \\ &\geq \cos\theta \big(|\Sigma_{SV}| + |\Sigma_{LV}| \big) \\ &\geq \cos\theta \big(|\Pi(\Sigma_{SV})| + |\Pi(\Sigma_{LV})| \big) \geq \cos\theta |Q_r| \ , \end{aligned}$$

where Π denotes the orthogonal projection of $\mathbb{R}^d$ onto the horizontal plane $x_d = 0$, the second inequality follows from the fact that orthogonal projections reduce area, and the

last inequality follows by the fact that the projections of Σ_{SV} or Σ_{LV} cover Q_r, that is, every vertical line passing through Q_r meets either Σ_{SV} or Σ_{LV} at least once.

4.2. Upper bounds for $\cos\theta^{\rm hom}$. - By formula (4.2), the energy of an admissible test configuration $L^{\rm trial}$ gives an *upper bound* on $\cos\theta^{\rm hom}$, and precisely

$$\cos\theta^{\rm hom} \le \frac{\tilde E(L^{\rm trial}, C_r)}{|Q_r|} \ . \tag{4.3}$$

We show below that Wenzel and Cassie-Baxter laws correspond to particular choices of the test configuration $L^{\rm trial}$, and therefore give two upper bounds for $\cos\theta^{\rm hom}$. As pointed out in §4.6, for certain geometries none of these bounds is attained, and both laws overestimate the enhancement of hydrophilicity (or hydrophobicity) due to roughness.

4.3. Wenzel bound. - By taking $L^{\rm trial}$ empty, we get $\tilde E(L^{\rm trial}, C_r)$ equal to $\cos\theta\,|\partial S_1 \cap C_r| = \cos\theta\, R|Q_r|$, which gives the Wenzel bound

$$\cos\theta^{\rm hom} \le R\cos\theta \ .$$

This bound is achieved when there is perfect contact between the solid and vapor phases, which is the assumption of Wenzel's model. This is indeed the case for $\cos\theta$ small enough (see §4.5 and §4.6).

4.4. Cassie-Baxter bound. - Let m be the maximal height for a point in S_1, that is, $P_m := \{x :\ x_d \le m\}$ is the smallest horizontal half-space that contains S_1. Now we take the configuration $L^{\rm trial} := (P_m \setminus S_1) \cap C_r$ (see Figure 4) to obtain an upper bound for $\cos\theta^{\rm hom}$ as in (4.3).

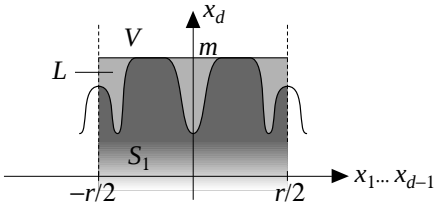

Fig. 4. Trial configuration for the Cassie-Baxter bound (hydrophilic case).

In this case Σ_{SV} and Σ_{LV} are a partition of the square Q_r (translated to height m), and hence $|\Sigma_{SV}| + |\Sigma_{LV}| = |Q_r|$. Setting

$$\phi_s := \frac{|\{x \in Q_r :\ f(x) = m\}|}{|Q_r|} \ , \tag{4.4}$$

we have $\tilde E(L^{\rm trial}, C_r) = \cos\theta\,|\Sigma_{SV}| + |\Sigma_{LV}| = \big(\phi_s\,\cos\theta + 1 - \phi_s\big)|Q_r|$. Hence we obtain the Cassie-Baxter bound

$$\cos\theta^{\rm hom} \le \phi_s\cos\theta + 1 - \phi_s \ .$$

For special geometries, this bound is actually achieved if $\cos\theta$ is large enough (see §4.6).

The hydrophobic case

All the arguments used in the previous subsection have a natural counterpart in the hydrophobic case, $\cos\theta \le 0$. We give a complete review of the results for the convenience of the reader, but we will omit proofs since these are immediately obtained from those in the hydrophilic case by replacing $\cos\theta$ with $|\cos\theta|$, and exchanging the role of the phases L and V.

Using the renormalized energy $\tilde{E}$ given in (2.8), we obtain the formula

$$-\cos\theta^{\rm hom} = |\cos\theta^{\rm hom}| = \tilde{\sigma}_{SL}^{\rm hom} = \inf_{V} \frac{1}{|Q_r|}\tilde{E}(V, C_r) \ , \tag{4.5}$$

where the class of admissible V is the same as for the cell problem (3.5), see Section 3. As before, roughness always enhances hydrophobicity, namely,

$$|\cos\theta| \le |\cos\theta^{\rm hom}| \ .$$

An upper bound for $|\cos\theta^{\rm hom}|$ can be obtained from (4.5) by using an arbitrary admissible test configuration $V^{\rm trial}$. Taking for $V^{\rm trial}$, respectively, the empty set and the configuration obtained from Figure 4 by exchanging the roles of L and V we obtain the Wenzel and Cassie-Baxter bounds

$$|\cos\theta^{\rm hom}| \le R|\cos\theta| \quad \text{and} \quad |\cos\theta^{\rm hom}| \le \phi_s|\cos\theta| + 1 - \phi_s \ ,$$

where the geometric parameters R and ϕ_s are defined in (4.1) and (4.4).

Further remarks

4.5. Achievement of the Wenzel bound. - Let S_1 be the subgraph of a regular function f (cf. (3.2)). Then the Wenzel bound is achieved for

$$|\cos\theta| \le \frac{1}{\sqrt{1+m^2}} \quad \text{where } m := \max_{x\in Q_r} |\nabla f(x)| \ .$$

We prove this assertion in the hydrophilic case. Consider an admissible test configuration L for the minimum problem in (4.2). Then

$$\begin{aligned}
\cos\theta\,|\Sigma_{SL}| &\le \frac{|\Sigma_{SL}|}{\sqrt{1+m^2}} \\
&= \frac{1}{\sqrt{1+m^2}} \int\limits_{\Pi(\Sigma_{SL})} \sqrt{1+|\nabla f|^2} \\
&\le |\Pi(\Sigma_{SL})| = |\Pi(\Sigma_{LV})| \le |\Sigma_{LV}| \ ,
\end{aligned}$$

where Π is the projection onto the plane $x_d = 0$, the last equality follows from the fact that Σ_{SL} and Σ_{LV} have the same projection, and the last inequality from the fact that orthogonal projections reduce the area. Using the inequality above,

$$\begin{aligned}
\tilde{E}(L, C_r) &= \cos\theta\,|\Sigma_{SV}| + |\Sigma_{LV}| \\
&= \cos\theta\,\big(|\partial S_1 \cap C_r| - |\Sigma_{SL}|\big) + |\Sigma_{LV}| \\
&\ge \cos\theta |\partial S_1 \cap C_r| = R\cos\theta\,|Q_r| \ ,
\end{aligned}$$

which implies, by (4.2), $\cos\theta^{\rm hom} \geq R\cos\theta$, that is, Wenzel bound is achieved.

4.6. EXAMPLES. - Depending on the geometry and on $\cos\theta$, the macroscopic coefficient $\cos\theta^{\rm hom}$ can agree with the Wenzel bound, with the Cassie-Baxter bound, or with none of the two. Examples of these situations in the hydrophobic case and for $d = 2$ are described in Figure 5. For the geometry in (A) or (B), the Wenzel bound is attained when

$$\frac{a}{b} \leq \frac{1 - |\cos\theta|}{2|\cos\theta|} \,,$$

(and the geometric parameter R is equal to $1 + 4a/r$) while the Cassie-Baxter bound is attained in the remaining cases (and $\phi_s = 1 - 2b/r$).

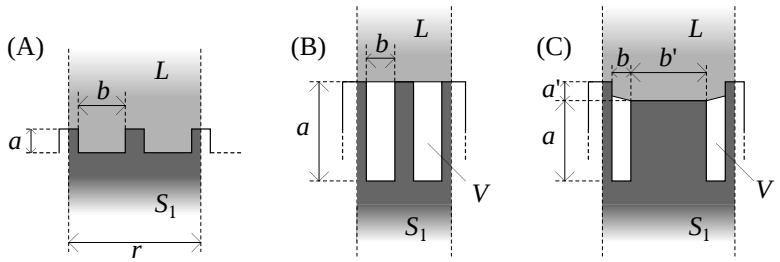

FIG. 5. Examples of optimal configurations in the hydrophobic case: (A) Wenzel, (B) Cassie-Baxter, (C) mixed.

The geometry in (C) leads to a more interesting behavior.[(2)] The configuration displayed in the figure mixes features of Wenzel's (complete contact on tall asperities) with features of the Cassie-Baxter ones (composite contact on short asperities). To simplify computations, it is convenient to estimate its energy from above by replacing the slightly tilted liquid-vapor interfaces in Figure 5(C) with horizontal ones. It is then easy to show that the mixed configuration is the optimal one if

$$\frac{a'}{b'} \leq \frac{1 - |\cos\theta|}{2|\cos\theta|} \leq \frac{a}{b} \,.$$

If this is the case, the Wenzel and Cassie-Baxter laws overestimate the value of $|\cos\theta^{\rm hom}|$, respectively by

$$\frac{4a|\cos\theta| - 2b(1 - |\cos\theta|)}{r} \quad \text{and} \quad \frac{b'(1 - |\cos\theta|) - 2a'|\cos\theta|}{r} \,.$$

4.7. CONCLUSIONS. - The results of this section are summarized in Figure 6 below. In contrast with statements that are found in the literature, the plot shows that it is not

(2) Cassie-Baxter law is usually discussed for rough surfaces with only one type of asperities. For surfaces mixing tall and short asperities, there is not a unique way of realizing a composite contact. Our definition of Cassie-Baxter configurations aims at ensuring that the parameter ϕ_s appearing in the Cassie-Baxter laws for the contact angle depend only on the geometry of the surface, and not on features of the equilibrium configuration (which is a–priori unknown).

possible to turn a hydrophilic surface into a hydrophobic one by tuning its roughness. Of course, this does not exclude that a drop on a rough hydrophilic surface may exhibit a contact angle larger than $\pi/2$. Configurations of this type are actually observed [16], but our results show that they are only metastable. Notice also that the graph in Figure 6 is symmetric under change of sign of $\cos\theta$, while calculations leading to non-symmetric diagrams are often reported in the literature. Also for this discrepancy, the explanation lies in metastability: The equilibrium configurations analyzed, e.g., in [4], leading to a non-symmetric relation $\cos\theta \mapsto \cos\theta^{\rm hom}$, are not energy minimizing in the small $\cos\theta$ regime where the Wenzel bound is always attained (this fact is actually confirmed by the experiments in [16]). Finally, another interesting consequence of our analysis is a selection criterion for energy optimality: lowest energy is associated with smallest $|\cos\theta^{\rm hom}|$, i.e., with the most conservative estimate of the roughness-induced enhancement of the hydrophobic or hydrophilic properties of a surface.

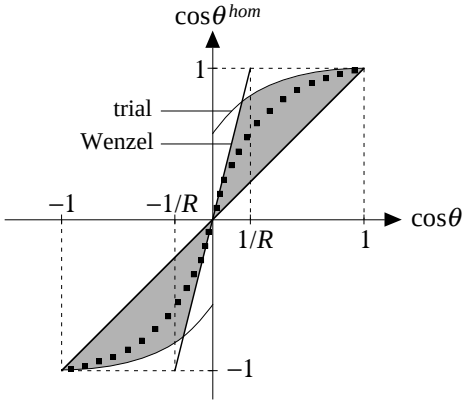

FIG. 6. Plot of a typical relation $\cos\theta \mapsto \cos\theta^{\rm hom}$ for a given geometry (dotted curve). Points corresponding to minimum energy configurations must lie in the shaded area, delimited by the bounds given in the text.

5. Rigorous mathematical result

We define Q_r, C_r, and S_ε as in Section 3, except that we do not assume any symmetry for S_1. The solid-liquid and solid-vapor interfacial energy densities are functions on ∂S_ε which depends on ε as described in (3.7).

The ambient space is a bounded open set Ω of $\mathbb{R}^d$; each configuration of the system associated to S_ε is described by a subset L of Ω which does not intersects S_ε, or by its complement $V := \Omega \setminus (S_\varepsilon \cup L)$. The energy of a configuration L within the container Ω is

$$E_\varepsilon(L) = E_\varepsilon(L,\Omega) := \int\limits_{\Sigma_{SL}\cap\Omega} \sigma^\varepsilon_{SL} \; + \int\limits_{\Sigma_{SV}\cap\Omega} \sigma^\varepsilon_{SV} \; + \sigma_{LV}|\Sigma_{LV}\cap\Omega| \; . \tag{5.1}$$

For technical reasons, it is convenient to encode the constraint $L \cap S_\varepsilon = \varnothing$ in the functional, by setting $E_\varepsilon(L) := +\infty$ for all sets $L \subset \Omega$ that intersect S_ε.

5.1. Additional requirements and remarks. - (i) Volume and volume integrals are computed in term of the Lebesgue measure $\mathscr{L}^d$, while surface areas and surface integrals, like those in (5.1), are computed in terms of the $(d-1)$-dimensional Hausdorff measure $\mathscr{H}^{d-1}$. Sets and functions are always assumed to be Borel measurable.

(ii) We denote by $\mathscr{X}$ the class of all Borel subsets of Ω. On this class, we consider the distance given by the volume of the symmetric difference, that is

$$\operatorname{dist}(A,B) := |A \setminus B| + |B \setminus A| \ . \tag{5.2}$$

In this context, we identify sets which differ by a Lebesgue-null subset.

(iii) The solid-liquid interface Σ_{SL} is intended as the *essential common boundary* of the sets S_ε and L, namely the set of all points in Ω where both sets have strictly positive lower d-dimensional density. The interfaces Σ_{SV} and Σ_{LV} are defined in a similar way. We also assume that the *essential* boundary of the set S_1, namely the set of all points in $\mathbb{R}^d$ where both S_1 and its complement have strictly positive lower density, has locally finite area.

(iv) The interfaces Σ_{SL} and Σ_{SV} are contained in the essential boundary of S_ε, and therefore have always finite area. If the liquid-vapor interface Σ_{LV} has finite area, or, equivalently, if the energy $E_\varepsilon(L,\Omega)$ is finite, then L is a set with finite perimeter in Ω in the sense of Caccioppoli, and the perimeter agrees with the sum of the areas of the solid-liquid and liquid-vapor interfaces (cf. [10], §5.8, Lemma 1).

(v) When the boundary of L is piecewise smooth, the notion of interface given above agrees with the familiar one. However, since our variational approach is based on compactness and semicontinuity methods, it is convenient to consider a class of sets L which is large enough to enjoy some "easy" compactness property, such as the class of finite perimeter sets. From this viewpoint, the right notion of area of an interface is exactly the $(d-1)$-dimensional Hausdorff measure of the essential common boundary of the two phases. Indeed, the perimeter of L, and the total interfacial energy $E_\varepsilon(L)$ are lower semicontinuous on $\mathscr{X}$ (the semicontinuity of E_ε requires that the interfacial energy densities satisfy the wetting condition (2.2), cf. [2], Remark 2.5). In particular, it follows from the standard compactness theorem for finite perimeter sets (cf. [3], Theorem 3.39) that the minimum of E_ε among all sets L with prescribed volume l is achieved; the same holds even if we add to E_ε an additional term which is lower semicontinuous on $\mathscr{X}$, such as the potential energy (2.3).

5.2. Theorem. - (i) *The functionals E_ε are uniformly coercive on $\mathscr{X}$, i.e., every sequence of sets (L_ε) with bounded energies $E_\varepsilon(L_\varepsilon)$ is pre-compact in $\mathscr{X}$.*

(ii) *As $\varepsilon \to 0$, E_ε Γ-converge on $\mathscr{X}$ to the functional $E^{\hom}$ given by*

$$E^{\hom}(L) := \sigma_{SL}^{\hom}|\Sigma_{SL}| + \sigma_{SV}^{\hom}|\Sigma_{SV}| + \sigma_{LV}|\Sigma_{LV}|$$

for every $L \in \mathscr{X}$ which does not intersects $S := \{x_d \le 0\}$, and extended to $+\infty$ otherwise, where

$$\sigma_{SL}^{\hom} := \liminf_{n\to\infty} \left\{ \inf_V \frac{E_1(V, C_{nr})}{|Q_{nr}|} \right\} , \quad \sigma_{SV}^{\hom} := \liminf_{n\to\infty} \left\{ \inf_L \frac{E_1(L, C_{nr})}{|Q_{nr}|} \right\} \tag{5.3}$$

and the infima are taken over all bounded sets V (respectively, L) contained in C_{nr} which do not intersect S_1.

(iii) *If the set S_1 is symmetric with respect to the coordinate planes $x_i = 0$ for $i = 1, \dots, d-1$, then $\sigma_{SL}^{\rm hom}$ and $\sigma_{SV}^{\rm hom}$ are given by formulas* (3.4) *and* (3.5), *respectively.*

(iv) *For every $\varepsilon > 0$, let L_ε be a minimizer of $E_\varepsilon(L)$ with prescribed volume $|L| = l$. Then the sequence (L_ε) is pre-compact in $\mathscr{X}$, and every limit point is a minimizer of $E^{\rm hom}(L)$ with prescribed volume $|L| = l$.*

5.3. Remarks. - (i) For details on the notion of Γ-convergence and its applications, we refer the reader to [1], [7].

(ii) Statement (i) is an immediate consequence of the standard compactness result for finite perimeter sets, cf. §5.1(v).

(iii) The existence of minimizers in statement (iv) is ensured by standard lower semicontinuity and compactness arguments, provided that $l < |\Omega \setminus S_\varepsilon|$, cf. §5.1(v). Their compactness follows from statement (i), while the convergence to a minimizer of $E^{\rm hom}$ is a standard corollary of the Γ-convergence of the energies. More precisely, we need the Γ-convergence of E_ε to $E^{\rm hom}$ on the subclass of all $L \in \mathscr{X}$ with prescribed volume $|L| = l$. We omit to prove this easy variant of statement (ii).

(iv) Since Γ-convergence is stable under continuous perturbations, statement (ii) and (iv) holds even if we add to the energies an additional term which is continuous on $\mathscr{X}$, such as the potential energy (2.3).

The rest of this section is devoted to the proof of statements (ii) and (iii); since they are quite standard, we only sketch them. Statement (ii) consists of two separate parts: the lower bound inequality and the upper bound inequality.

5.4. Proof of the lower bound inequality. - In the following we will freely pass to subsequence without relabelling. We must show that if L_ε converge to L in $\mathscr{X}$, then

$$\liminf_{\varepsilon \to 0} E_\varepsilon(L_\varepsilon) \geq E^{\rm hom}(L) \ . \tag{5.4}$$

We can assume that the lower limit is finite, and is actually a limit. We denote by λ_ε the energy distributions in Ω associated to the energies E_ε and the configurations L_ε. Up to subsequence, λ_ε converge in the sense of measures to some finite measure λ, and by a standard argument (first given in [12]), to prove (5.4) it suffices to show that the $(d-1)$-dimensional density of λ satisfies

$$\mathrm{dens}_{d-1}(\lambda, x) \geq \sigma_{LV} \quad \text{for a.e. } x \in \Sigma_{LV}, \tag{5.5}$$

$$\mathrm{dens}_{d-1}(\lambda, x) \geq \sigma_{SV}^{\rm hom} \quad \text{for a.e. } x \in \Sigma_{SV}, \tag{5.6}$$

$$\mathrm{dens}_{d-1}(\lambda, x) \geq \sigma_{SL}^{\rm hom} \quad \text{for a.e. } x \in \Sigma_{SL}. \tag{5.7}$$

Inequality (5.5) is a straightforward consequence of the lower semicontinuity of perimeter. The proof of inequality (5.6) is more delicate. Let $U(x, \rho)$ denote the d-dimensional cube with center x, side of length ρ, and axis parallel to the coordinate axis. For a.e. $x \in \Sigma_{SV}$, the $(d-1)$-dimensional density of λ at x is given by

$$\mathrm{dens}_{d-1}(\lambda, x) = \lim_{i \to \infty} \frac{\lambda(U(x, \rho_i))}{\rho_i^{d-1}} \ ,$$

where ρ_i is any sequence converging to 0. By choosing ρ_i so that $\lambda(\partial U(x, \rho_i)) = 0$, we have that $\lambda(U(x, \rho_i))$ is the limit as $\varepsilon \to 0$ of $\lambda_\varepsilon(U(x, \rho_i)) = E_\varepsilon(L_\varepsilon, U(x, \rho_i))$, and by a

standard diagonal argument we can choose ε_i so that $\varepsilon_i \to 0$ and

$$\mathrm{dens}_{d-1}(\lambda, x) = \lim_{i\to\infty} \frac{E_{\varepsilon_i}(L_{\varepsilon_i}, U(x,\rho_i))}{\rho_i^{d-1}} \ . \tag{5.8}$$

We can also choose ε_i so that $\varepsilon_i \ll \rho_i$, and ρ_i/ε_i is a number of the form $n_i r$ with n_i integer (converging to $+\infty$). Let now T_i be an homothety with scaling factor $1/\varepsilon_i$ which takes $U(x,\rho_i)$ into $U_i := U(0, n_i r)$, and set $L_i' := T_i(L_{\varepsilon_i}) \cap U_i$. Then

$$\frac{E_{\varepsilon_i}(L_{\varepsilon_i}, U(x,r_i))}{\rho_i^{d-1}} = \frac{E_1(L_i', U_i)}{(n_i r)^{d-1}} \ . \tag{5.9}$$

Since the d-dimensional density L at x is 0 for a.e. $x \in \Sigma_{SV}$, we can choose the numbers ρ_i and ε_i so that, in addition, $|L_i'| \ll |U_i| = (n_i r)^d$. Therefore, taking the truncated sets $L_i'' := L_i' \cap \{x_d \le t_i\}$ with suitably chosen $0 < t_i < n_i r/2$, the total interfacial energy associated to L_i'' satisfies

$$E_1(L_i'', C_{n_i r}) = E_1(L_i'', U_i) = E_1(L_i', U_i) + o((n_i r)^{d-1}) \ . \tag{5.10}$$

Putting together (5.8), (5.9), (5.10), and the definition of $\sigma_{SV}^{\mathrm{hom}}$ in (5.3), we obtain

$$\mathrm{dens}_{d-1}(\lambda, x) = \lim_{i\to\infty} \frac{E_1(L_i'', C_{n_i r})}{(n_i r)^{d-1}} \ge \sigma_{SV}^{\mathrm{hom}} \ .$$

The proof of (5.7) is identical. □

5.5. Proof of the upper bound inequality. - By standard arguments, proving the upper bound inequality reduces to show the following: given a positive number δ and a set L in $\Omega \setminus S$ with piecewise smooth boundary such that Σ_{LV} meets ∂S transversally, there exists a sequence of sets (L_ε) converging to L such that

$$\limsup_{\varepsilon\to 0} E_\varepsilon(L_\varepsilon) \le E^{\mathrm{hom}}(L) + \delta \ .$$

By the definition of homogenized coefficients, we can choose m and $V_\delta \subset C_{mr} \setminus S_1$, and n and $L_\delta \subset C_{nr} \setminus S_1$, so that

$$\frac{E_1(V_\delta, C_{mr})}{|Q_{mr}|} \le \sigma_{SL}^{\mathrm{hom}} + \delta \ , \quad \frac{E_1(L_\delta, C_{nr})}{|Q_{nr}|} \le \sigma_{SV}^{\mathrm{hom}} + \delta \ .$$

For ε sufficiently small we construct the configuration L_ε by perturbing L as shown in Figure 7 below.

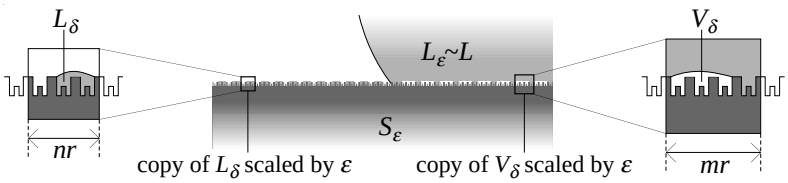

Fig. 7. Construction of L_ε by scaled copies of V_δ and L_δ.

Clearly L_ε converge to L as $\varepsilon \to 0$, and a simple computation yields the estimate $\limsup E_\varepsilon(L_\varepsilon) \le E^{\hom}(L) + O(\delta)$. □

5.6. PROOF OF STATEMENT (iii). - We have to show that the right-hand side of (3.4) is equal to the right-hand side of the first equality in (5.3). It is clear that the former is not larger than the latter. To prove the opposite inequality, it suffices to show that for every integer n and every set $V \subset C_{nr} \setminus S_1$, we can find a symmetric set V' in $C_r \setminus S_1$ such that

$$\frac{E(V', C_r)}{|Q_r|} \le \frac{E(V, C_{nr})}{|Q_{nr}|} \,. \tag{5.11}$$

To this end, we subdivide C_{nr} into $(2n)^{d-1}$ pairwise disjoint parallel copies C of the cylinder $(0, r/2)^{d-1} \times \mathbb{R}$ (a quarter of the periodicity cell C_r), and among them we choose the one which minimizes the energy $E(V, C)$. Hence $E(V, C) \le E(V, C_{nr})/(2n)^{d-1}$. By taking the union of 2^{d-1} copies of $V \cap C$, suitably reflected and translated, we obtain a symmetric set V' in $C_r \setminus S_1$ such that $E(V, C_r) = 2^{d-1} E(V, C) \le E(V, C_{nr})/n^{d-1}$, and therefore V' satisfies (5.11).

In a similar way, one proves that the right-hand side of (3.5) is equal to the right-hand side of the second equality in (5.3). □

Bibliography

1. G. Alberti: Variational models for phase transitions. An approach via Γ-convergence. *Differential equations and calculus of variations. Topics on geometrical evolution problems and degree theory (Pisa 1996)*, 95-114. G. Buttazzo et al. Eds. Springer, Berlin, 2000.
2. G. Alberti, G. Bouchitté, P. Seppecher: Phase transition with line-tension effect. *Arch. Rational Mech. Anal.*, **144** (1998), 1-46.
3. L. Ambrosio, N. Fusco, D. Pallara: *Functions of bounded variation and free discontinuity problems*. Oxford Mathematical Monographs. Oxford Science Publications, Oxford, 1999
4. J. Bico, C. Marzolin, and D. Quéré: Pearl drops. *Europhysics Letters A*, **47** (1999), 220-226.
5. J. Bico, U. Thiele, D. Quéré: Wetting of textured surfaces. *Colloids and Surfaces A*, **206** (2002), 41-46.
6. R. Blossey: Self-cleaning surfaces - virtual realities. *Nature Materials*, **2** (2003), 301-306.
7. A. Braides: *Γ-convergence for beginners*. Oxford Lecture Series in Mathematics and its Applications, 22. Oxford University Press, Oxford, 2002.
8. A.B. Cassie, S. Baxter: Wettability of porous surfaces. *Trans. Faraday Soc.*, **40** (1944), 546-551.
9. A. Checco, P. Guenoun, J. Daillant: Nonlinear Dependence of the Contact Angle of Nanodroplets on Contact Line Curvature. *Phys. Rev. Letters*, **91** (2003), 18601.
10. L.C. Evans, R.F. Gariepy: *Measure theory and fine properties of functions*. Studies in Advanced Mathematics, CRC Press, Boca Raton 1992.
11. R. Finn: *Equilibrium capillary surfaces*. Springer, New York 1986.
12. I. Fonseca, S. Müller: Relaxation of quasiconvex functionals in $BV(\Omega, \mathbb{R}^p)$ for integrands $f(x, u, \nabla u)$. *Arch. Rat. Mech. Anal.*, **123** (1993), 1-49.
13. P.-G. de Gennes, F. Brochard-Wyart, D. Quéré: *Capillarity and wetting phenomena*. Springer-Verlag, New York, 2004.

14. S. Herminghaus: Roughness-induced non-wetting. *Europhys. Lett.*, **52** (2000), 165-170.
15. R.E. Johnson, R.H. Dettre: Contact angle hysteresis. In: *Contact angle, wettability, and adhesion.* Advances in Chemistry Series, **43** (1964), 112-135.
16. A. Lafuna, D. Quéré: Superhydrophobic states. *Nature Materials*, **2** (2003), 460-463.
17. K.K.S. Lau, J. Bico, K.B.K. Teo, M. Chhowalla, G.A.J. Amaratunga, W.I. Milne, G.H. McKinley, K.K. Gleason: Superhydrophobic carbon nanotube forests. *Nano Letters*, **3** (2003), 1701-1705.
18. C. Neinhuis, W. Barthlott: Purity of the sacred lotus, or escape from contamination in biological surfaces. *Planta*, **202** (1997), 1-8.
19. C. Neinhuis, W. Barthlott: Characterization and distribution of water-repellent, self-cleaning plant surfaces. *Ann. Bot.*, **79** (1997), 667-677.
20. N.A. Patankar: On the modeling of hydrophobic contact angles on rough surfaces. *Langmuir*, **19** (2003), 1249-1253.
21. D. Quéré: Model droplets. *Nature Materials*, **3** (2004), 79-80.
22. P.S. Swain, R. Lipowsky: Contact angles on heterogeneous surfaces: A new look at Cassie's and Wenzel's Laws. *Langmuir*, **14** (1998), 6772-6780.
23. R.N. Wenzel: Resistence of solid surfaces to wetting by water. *Ind. Eng. Chem.*, **28** (1936), 988-994.

Giovanni Alberti: Dipartimento di Matematica, Università di Pisa, via Buonarroti 2, 56127 Pisa, Italy (e-mail: alberti@dm.unipi.it).

Antonio DeSimone: SISSA - International School for Advanced Studies, via Beirut 4, 34014 Trieste, Italy (e-mail: desimone@sissa.it)